ELSEVIER

Chemical Engineering Journal 133 (2007) 85–95

Chemical Engineering Journal

www.elsevier.com/locate/cej

Solid phase hydrodynamics of three-phase fluidized beds—A convective/dispersive mixing model

Sylvain Lefebvre, Christophe Guy *, Jamal Chaouki

Chemical Engineering Department, Ecole Polytechnique, P.O. Box 6079, St. "C.V." Montreal, Que., Canada H3C 3A7

Received 24 April 2006; received in revised form 3 February 2007; accepted 5 February 2007

Abstract

The main objective of this work was to develop a solid phase mixing model that followed not only the mixing extent, but also the overall mixing mechanism, i.e., the contribution of the convective onto the dispersive mixing mechanism. A non-invasive radioactive particle tracking (RPT) technique was used to estimate the model parameters and generate tracer curves at various axial positions. The proposed model follows the tracer data well compared to the axial dispersion model. It has the flexibility to represent various contributions of the convective onto the dispersive mixing mechanism observed in three-phase fluidized beds and it is linked to the bubble velocity distribution. The convective/dispersive model successfully followed the evolution of the extent of particle mixing and the overall mixing mechanism at various superficial gas and liquid velocities as well as reactor diameters.

Keywords: Three-phase fluidization; Solid mixing; Convective and dispersive mixing model

1. Introduction

Three-phase fluidized bed reactors are used in various industries, such as the petrochemical, biological and mineral industries. In order to design, optimize and scale-up three-phase fluidized bed reactors, models may be used. CFD models are great potential tools, but empirical closing equations and long computing times limit the utilization of such models. More simple models, called mixing models, which are based on assumptions about flow patterns, may be employed. These mixing models include the axial dispersion model, which is often relied on to model each phase without physical justification. Mixing models should be based on key hydrodynamic properties, such as mixing mechanisms, e.g., convective and dispersive mechanisms [1,2].

Lefebvre et al. [3] reviewed phenomenological mixing models proposed in the literature for reactors containing bubbles. The main conclusions were that the gas phase followed a convective mechanism [4], i.e., represented by a distribution of plug flow reactors in parallel. This means that bubbles are assumed to have constant Lagrangian rising velocities along the reactor length. This gives a convective mixing contribution to the liquid phase [5] due to the transport of the liquid in the bubble wake. Constant Lagrangian particle velocities were observed with radioactive particle tracking (RPT) measurements for the solid phase [6] due, also, to the transport of the solid particles into the bubble wake. Based on these key hydrodynamic properties, Lefebvre et al. [3] proposed an updated version of the structural wake model [7]. There is no solid phase mixing model that takes into account the convective mixing contribution coming from the bubble wake transport at *various* Lagrangian constant velocities.

Lefebvre et al. [8] relied on RPT data to compute parameters to investigate the relative contribution of the convective and dispersive mixing mechanisms on the overall solid phase mixing. One important finding was that the extent of mixing and the overall mixing mechanism (relative importance of the convective onto the dispersive mechanism) did not follow the same trend with experimental conditions, e.g., when the mixing extent increased, the relative importance of the convective mechanism might decrease or increase. A solid phase mixing model should follow not only the mixing extent, but also the overall mixing

* Corresponding author. Tel.: +1 340 4990; fax: +1 340 4992.
E-mail address: christophe.guy@polymtl.ca (C. Guy).

1385-8947/$ – see front matter © 2007 Published by Elsevier B.V.
doi:10.1016/j.cej.2007.02.004

Nomenclature

A	area of the solid phase, $(D_c^2\pi/4)\varepsilon_s$ (m^2)
$C_{pde}\|_{u_{pded}}$	tracer concentrations in class defined by the particle velocity u_{pded} of the particle downflow-emulsion phase (kg/m^3) or normalized
C_{pve}	tracer concentration in the particle vortex-emulsion phase (kg/m^3) or normalized
$C_{pw}\|_{u_{pwd}}$	tracer concentration in the class defined by the particle velocity u_{pwd} of the particle wake phase (kg/m^3) or normalized
$C_{s\,exp}$	experimental tracer concentration; normalized
$C_{s\,mod}$	model tracer concentration; normalized
C_∞	tracer concentration at homogenization—tracer test in batch (kg/m^3)
$D_{ax_{eff}}$	apparent axial dispersion coefficient of the axial dispersion model (m^2/s)
$D_{ax_{pve}}$	axial dispersion coefficient of the particle vortex-emulsion phase (m^2/s)
D_c	column diameter (m)
$f\{u_{pded}\}$	solid velocity distribution of the particle downflow-emulsion phase (s/m)
$f\{u_{pwd}\}$	solid velocity distribution of the particle wake phase (s/m)
$K_{pde–pve}$	proportional constant for the exchange from particle downflow-emulsion phase to particle vortex-emulsion phase (s^{-1})
$K_{pve–pde}$	proportional constant for the exchange from particle vortex-emulsion phase to particle downflow-emulsion phase (s^{-1})
$K_{pve–pw}$	proportional constant for the exchange from particle vortex-emulsion phase to particle wake phase (s^{-1})
$K_{pw–pve}$	proportional constant for the exchange from particle wake phase to particle vortex-emulsion phase (s^{-1})
L_f	fluidized bed height (m)
MMI	mixing mechanism index, $(\phi_{pw}\sigma_{pwd} + \phi_{pde}\sigma_{pded})/\phi_{pve}\sigma_{pved}$
Nb_t	number of time steps
Nb_z	number of axial measurement positions
r^2	normalized square residual
t	time (s)
Δt	time step (s)
u_{pde}	mean particle velocity of the velocity distribution for the downflow-emulsion phase (m/s)
u_{pded}	solid velocity in class defined by particle velocity u_{pded} of the particle downflow-emulsion phase (m/s)
u_{pw}	mean particle velocity of the velocity distribution for the wake phase (m/s)
u_{pwd}	solid velocity in class defined by particle velocity u_{pwd} of the particle wake phase (m/s)
z	axial position (m)
Δz	axial length step (m)

Greek letters

α	parameter of the log-normal distribution function
β	parameter of the log-normal distribution function
ε_s	solid fraction
ϕ_{pde}	particle downflow-emulsion phase holdup
ϕ_{pve}	particle vortex-emulsion phase holdup
ϕ_{pw}	particle wake phase holdup
σ_{pwd}	standard deviation of the velocity distribution for the downflow-emulsion phase (m/s)
σ_{pwd}	standard deviation of the velocity distribution for the wake phase (m/s)

mechanism. The objective of this work was to develop such a mixing model.

2. Experimental

2.1. Experimental setups and operating conditions

Data were obtained from two different size co-current upward three-phase fluidized bed reactors and for various particle systems. Water was used as the fluidized medium and air was the gas phase. Experiments were conducted at ambient temperature and pressure.

The smaller column had a diameter of 0.10 m. RPT data obtained in this column have already been published in previous articles, e.g., Larachi et al. [9], Larachi et al. [6], Cassanello et al. [10], Kiared et al. [11]. In a new, larger, three-phase fluidized bed, 0.292 m in diameter, nine new sets of RPT data were obtained. In total, 15 sets of RPT data were used here. Table 1 shows the experimental conditions. The range of superficial gas and liquid velocities was 0.010–0.106 and 0.042–0.065 m/s, respectively. Table 1 lists some particle properties. The 0.10 and 0.292 m columns had a height of 1.5 and 2.7 m, respectively. Description of the distribution systems and more details can be found in Lefebvre et al. [8].

2.2. Radioactive particle tracking (RPT)

Our noninvasive radioactive particle tracking (RPT) technique was used [12]. This technique followed one radioactively marked particle having the same diameter and density as the bed particles. The 3D position of the particle versus time was measured. Solid parameters, such as particle velocities and particle phase holdup, could then be computed to study solid phase hydrodynamics.

The RPT technique consisted of arranging various 76 mm × 76 mm uncollimated and unshielded NaI(TI) cylindrical scintillation detectors around the studied reactor. Eight detectors were used for the 0.10 m column and 16 for the 0.292 m column. A ^{46}Sc filled particle was used as the traced particle and had the same diameter and density as the bed particles. The ^{46}Sc was obtained using neutron radioactive capture by ^{45}Sc in the Ecole Polytechnique Slowpoke nuclear reactor. Radioactivity

Table 1
Experimental conditions

Run (#)	U_L (m/s)	U_g (m/s)	Particle system[a]	Total bed mass[b] (kg)	$\text{Umf}_{U_g} = 0$[c] (m/s)	u_t[d] (m/s)
$D_c = 0.10$ m						
1	0.065	0.032	GB3	4.0	0.036	0.37
2	0.065	0.069	GB3	4.0	0.036	0.37
3	0.065	0.106	GB3	4.0	0.036	0.37
4	0.065	0.106	{GB3}GB0.9	2.8	{0.036}0.009	{0.37}0.14
5	0.065	0.032	{GB3}GB5	3.0	{0.036}0.051	{0.37}0.47
6	0.065	0.032	GB3{GB5}	3.0	0.036{0.051}	0.37{0.47}
$D_c = 0.292$ m						
7	0.042	0.031	GB3	88	0.036	0.37
8	0.042	0.050	GB3	88	0.036	0.37
9	0.042	0.080	GB3	88	0.036	0.37
10	0.051	0.031	GB3	88	0.036	0.37
11	0.051	0.051	GB3	88	0.036	0.37
12	0.051	0.080	GB3	88	0.036	0.37
13	0.062	0.031	GB3	88	0.036	0.37
14	0.062	0.051	GB3	88	0.036	0.37
15	0.062	0.080	GB3	88	0.036	0.37

[a] GB: glass beads. The attached number represents the particle diameter in mm. {}: tracked particle.
[b] For binary system, the bulk volume ratio is approximately 1:1. The solid phase holdup at rest for glass beads particles is approximately 0.59.
[c] The liquid/solid minimum fluidization velocity was calculated by the Grace's [25] correlation.
[d] The terminal particle velocity was calculated by the Schiller and Naumann's [26] correlation.

of the ^{46}Sc was 50 and 200μCi for the 0.10 and the 0.292 m columns, respectively. The γ-rays emitted by the ^{46}Sc were detected by the scintillation detectors. A detector photon count depends on the traced particle location in the bed, the corresponding subtended effective solid angle and the bed attenuation. This triangulation technique was used to yield the instantaneous traced particle position at 30 ms intervals. Data were collected over 5–6 h for each experiment.

Prior to each experiment, the bed was fluidized and a set of measurements of the γ-ray photon count was made to calibrate the system using the traced particle rigidly positioned at 150 representative and known locations throughout the bed. Three parameters were fitted for each experiment: the linear attenuation coefficient of the gas–liquid–solid emulsion, the detectors dead time and the source radioactivity.

2.3. Mixing data from RPT

A tracer concentration curve generated after tracer injection was obtained from RPT data. This method assumed an ergodic motion process for the particles in the fluidized bed. It was already used by Cassanello et al. [13] to obtain, as was done here, pulsed tracer data. The injection region was below 0.2 m in the axial direction (close to the distributor). Several radioactive particle trajectories starting below 0.2 m were collected. The positions of the collected trajectories were followed over 10–30 s. The first position of the collected trajectories was set at zero. At each time step (0.03 s), the number of particles in various axial regions, for example $0 < z \leq 0.2$ and $0.2 < z \leq 0.4$, was counted and divided by the volume of the region. The tracer concentration at each time step was divided by the tracer concentration at homogenization. Normalized tracer curves were then obtained at various axial positions.

3. Convective/dispersive model development

3.1. Model concept

Based on the updated version of the structural wake model proposed by Lefebvre et al. [3] and the study of Lefebvre et al. [8], the solid phase mixing model shown in Fig. 1 is proposed. The solid phase is separated into three sub-phases, i.e., the particle wake phase, the particle downflow-emulsion phase and the vortex-emulsion phase. The dotted contours surround the particle phases. The solid in the particle wake phase is transported at the various bubble wake Lagrangian constant velocities, illustrated by the various boxes. This is demonstrated in Fig. 2, which gives an example of RPT data. The upward constant Lagrangian velocity paths are identified as the particle wake phase. Therefore, the solid follows the convective mixing mechanism in that particle phase. The emulsion phase is divided into two particle phases. The particle downflow-emulsion phase represents the

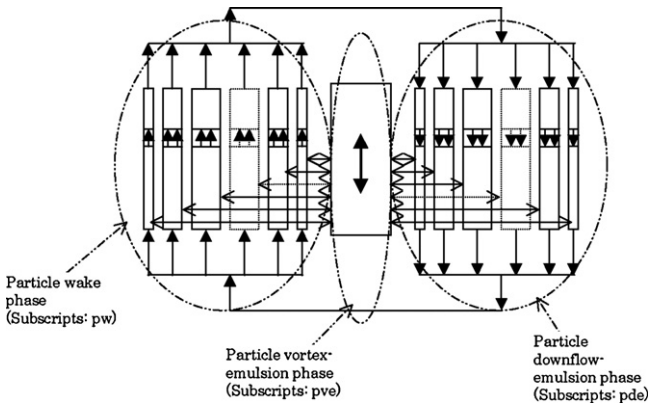

Fig. 1. Schematics of the solid phase convective/dispersive model.

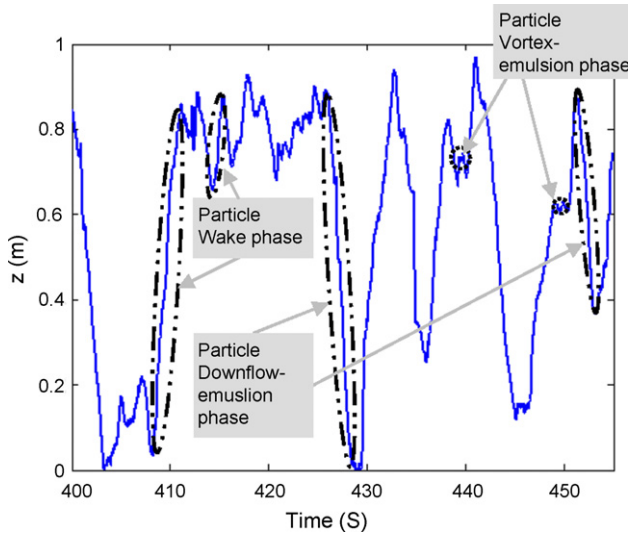

Fig. 2. Time series of the traced particle axial position. Particle phases examples. $D_c = 0.292$ m, GB3mm, $U_L = 0.042$ m/s, $U_g = 0.050$ m/s.

solid going down and following a convective mixing mechanism as a compensatory effect of the upward solid movement in the particle wake phase [6]. Therefore, the movement of the solid in the downflow-emulsion phase is indirectly linked to the gas phase hydrodynamics. The solid in the particle vortex-emulsion phase has a random movement, i.e., the particle position and velocity fluctuate erratically (dispersive mechanism). The solid in that particle phase is linked more to the liquid phase. Solid exchange occurs between the convective phases and the particle vortex-emulsion phase, but rarely between convective phases. Solid exchange is illustrated by the horizontal double arrows in Fig. 1. In Fig. 1, a large circulation pattern is represented by the arrow linking the convective phases at the top and bottom of the bed. This model agrees with the obvious superposition of the convective onto the dispersive mixing mechanism observed for the solid phase in three-phase fluidized bed reactors. It is also consistent with the result of Cassanello et al. [10] that the solid phase is superdispersive (faster than dispersive flow) in the axial direction.

3.2. Mathematical formulation

The model was applied onto a pulsed tracer test in batch mode constructed with the RPT data, as discussed previously. Mass balances on the solid phase convective/dispersive model were, therefore, made on an unsteady-state regime in a solid phase batch system.

The representation of multiple plug flows in parallel needed a velocity distribution function. Larachi et al. [6] and Lefebvre et al. [8] have shown that solid Lagrangian velocity distributions of the particle convective phases may be modelled after the log-normal distribution function shown in Eq. (1) for the particle wake phase. The Lagrangian velocity distribution of the particle wake phase may be viewed as the bubble velocity distribution. For the particle downflow-emulsion phase, replace u_{pwd}, u_{pw} and σ_{pwd} by u_{pded}, u_{pde} and σ_{pded}:

$$f\{u_{pwd}\} = \frac{1}{\beta u_{pwd}\sqrt{2\pi}} \exp\left[-\frac{(\ln(u_{pwd}) - \alpha)^2}{2\beta^2}\right] \quad (1)$$

The relations linking the mean (u_{pw}) and the standard deviation (σ_{pwd}) of the distribution to the function parameters (α, β) are shown in Eqs. (2) and (3):

$$u_{pw} = \exp\left(\alpha + \frac{\beta^2}{2}\right) \quad (2)$$

$$\sigma_{pwd} = \exp\left(\alpha + \frac{\beta^2}{2}\right)\sqrt{\exp(\beta^2) - 1} \quad (3)$$

Unsteady-state regime mass balance applied on a fraction of the solid in the particle wake phase rising at a velocity u_{pwd} (one of the plug flow reactors) is shown in the following equation.

$$\frac{\partial C_{pw}|_{u_{pwd}}}{\partial t} = -u_{pwd}\frac{\partial C_{pw}|_{u_{pwd}}}{\partial z} + K_{pw-pve}\left[C_{pve} - C_{pw}|_{u_{pwd}}\right] \quad (4)$$

With boundary conditions (B.C.):

$$C_{pw}\{z=0\} = \frac{\phi_{pde}}{\phi_{pw}}\frac{\int_0^\infty u_{pded} C_{pde}\{z=0, u_{pded}\} f\{u_{pded}\}\,du_{pded}}{\int_0^\infty u_{pded} f\{u_{pded}\}\,du_{pded}}$$

Several differential equations, like Eq. (4), have to be solved. The number of differential equations depends on the discretization of the log-normal velocity distribution. This number has to be high enough to converge to the solution of the system of equations (discussed later).

An equivalent equation is obtained for the solid in the particle downflow-emulsion phase:

$$\frac{\partial C_{pde}|_{u_{pded}}}{\partial t} = -u_{pded}\frac{\partial C_{pde}|_{u_{pded}}}{\partial z} + K_{pde-pve}\left[C_{pve} - C_{pde}|_{u_{pded}}\right] \quad (5)$$

$$\text{With B.C. : } C_{pde}\{z=L\} = \frac{\phi_{pw}}{\phi_{pde}}\frac{\int_0^\infty u_{pwd} C_{pw}\{z=L, u_{pwd}\} f\{u_{pwd}\}\,du_{pwd}}{\int_0^\infty u_{pwd} f\{u_{pwd}\}\,du_{pwd}}$$

Assuming that the solid mixing in the particle vortex-emulsion phase follows Fick's law, the unsteady-state regime mass balance gives:

$$\frac{\partial C_{pve}}{\partial t} = D_{ax_{pve}}\frac{\partial^2 C_{pve}}{\partial z^2} + \left(K_{pw-pve}\frac{\phi_{pw}}{\phi_{pve}}\right) \times \left[\int_0^\infty C_{pw} f\{u_{pwd}\}\,du_{pwd} - C_{pve}\right] + \left(K_{pde-pve}\frac{\phi_{pde}}{\phi_{pve}}\right) \times \left[\int_0^\infty C_{pded} f\{u_{pded}\}\,du_{pded} - C_{pve}\right] \quad (6)$$

$$\text{B.C.1}: \left.\frac{\partial C_{\text{pve}}}{\partial z}\right|_{z=0} = 0, \qquad \text{B.C.2}: \left.\frac{\partial C_{\text{pve}}}{\partial z}\right|_{z=L} = 0$$

The average solid tracer concentration is obtained by:

$$C_{\text{s}}\{z\} = \phi_{\text{pw}} \frac{\int_0^\infty u_{\text{pwd}} C_{\text{pw}}\{z, u_{\text{pwd}}\} f\{u_{\text{pwd}}\}\, \text{d}u_{\text{pwd}}}{\int_0^\infty u_{\text{pwd}} f\{u_{\text{pwd}}\}\, \text{d}u_{\text{pwd}}} + \phi_{\text{pde}} \frac{\int_0^\infty u_{\text{pded}} C_{\text{pde}}\{z, u_{\text{pded}}\} f\{u_{\text{pded}}\}\, \text{d}u_{\text{pded}}}{\int_0^\infty u_{\text{pded}} f\{u_{\text{pded}}\}\, \text{d}u_{\text{pded}}} + \phi_{\text{pve}} C_{\text{pve}} \tag{7}$$

Some explanations concerning the mass exchange terms have to be given. As a first formulation, the output flux of solid from one particle phase to another was assumed to be proportional to the concentration of the "expulsing" phase, e.g., output flux from the particle wake phase to the vortex-emulsion phase equal to $K_{\text{pw–pve}}\, C_{\text{pw}}|_{u_{\text{pwd}}}$. This assumption came from developments of Dayan and Zalmanovich [14], Turi and Ng [15], Tang and Fan [16] and Murray and Fan [17]. Depending on the authors, the value of $K_{\text{pw–pve}}$ is equal to the relative velocity of the particles close to the wake frontier, to the probability by unit length that the particles were discharged or to the axial velocity of the entrained particle. The total solid output flux from the particle vortex-emulsion phase to the wake phase was $K_{\text{pve–pw}} C_{\text{pve}}$. For one wake class defined by u_{pwd}, this total flux was weighted by the fraction of that class, i.e., $f\{u_{\text{pwd}}\}\, \text{d}u_{\text{pwd}}$. Therefore, the first formulation of Eq. (6) contained the following exchange term for the mass transfer between the particle wake phase and the particle vortex-emulsion phase:

$$\left[K_{\text{pw–pve}} \frac{\phi_{\text{pw}}}{\phi_{\text{pve}}} \left\{ \int_0^\infty C_{\text{pw}} f\{u_{\text{pw}}\}\, \text{d}u_{\text{pw}} \right\} - K_{\text{pve–pw}} C_{\text{pve}} \right] \tag{8}$$

At an infinite time, the net flux should be zero (Eq. (8) is equal to zero) for three-phase fluidized beds having a constant solid concentration axial profile. In other words, the tracer concentration was the same everywhere in the reactor. The following relation between the constants was then obtained:

$$K_{\text{pve–pw}} = K_{\text{pw–pve}} \frac{\phi_{\text{pw}}}{\phi_{\text{pve}}} \tag{9}$$

Replacing Eq. (9) with Eq. (8) gave the second term at the right of Eq. (6). The second term of Eqs. (4) and (5) as well as the third term of Eq. (6) were also obtained in that way.

3.3. Model parameters

Table 2 contains the model parameters and how they were obtained. The mean particle wake phase velocity (u_{pw}) was fitted using the model predictions of RPT tracer data. For the convective phases, it was observed that the dimensionless standard deviation ($\sigma_{\text{pwd}}/u_{\text{pw}}$ and $\sigma_{\text{pded}}/u_{\text{pde}}$) of the particle velocity distribution was only a function of the reactor diameter [8]. These simple relationships were used to evaluate the particle velocity distribution standard deviation (STD). The ratio of the particle mean velocities of the convective phases ($u_{\text{pde}}/u_{\text{pw}}$) was constant whatever the operating conditions, particle systems and reactor diameters. Particle vortex-emulsion phase holdup (ϕ_{pw}) was evaluated with RPT data [8]. Global mass balance linked the particle convective phases and made it possible to evaluate the particle downflow-emulsion phase holdup (ϕ_{pde}). Note that the mean particle velocity of the vortex-emulsion phase was zero. The particle vortex-emulsion phase holdup (ϕ_{pve}) was simply obtained by the definition of the holdup, i.e., $\phi_{\text{pw}} + \phi_{\text{pde}} + \phi_{\text{pve}} = 1$. The expanded bed height (L_{f}) was obtained from RPT data. The axial dispersion coefficient of the particle vortex-emulsion phase ($D_{\text{ax}_{\text{pve}}}$) and the exchange coefficient from the particle wake phase to the vortex-emulsion phase ($K_{\text{pw–pve}}$) were fitted using model predictions and experimen-

Table 2
Model parameters

Parameter	Unit	Evaluation[a]	Note
u_{pw}	m/s	Fitted	
σ_{pwd}	m/s	$\frac{\sigma_{\text{pwd}}}{u_{\text{pw}}} = 0.927 D_{\text{c}}^{0.355}$	Use $\sigma_{\text{pwd}}/u_{\text{pw}} = 0.49$ for run 15
u_{pde}	m/s	$\frac{u_{\text{pde}}}{u_{\text{pw}}} = 0.90$	
σ_{pded}	m/s	$\frac{\sigma_{\text{pded}}}{u_{\text{pde}}} = 0.873 D_{\text{c}}^{0.369}$	Use $\sigma_{\text{pded}}/u_{\text{pde}} = 0.48$ for run 15
ϕ_{pw}	–	RPT data	
ϕ_{pde}	–	$\phi_{\text{pde}} = \frac{u_{\text{pw}}}{u_{\text{pde}}} \phi_{\text{pw}}$	Global mass balance
ϕ_{pve}	–	$\phi_{\text{pve}} = 1 - \phi_{\text{pw}} - \phi_{\text{pde}}$	
L_{f}	m	RPT data	
$D_{\text{ax}_{\text{pve}}}$	m^2/s	Fitted	
$K_{\text{pw–pve}}$	s^{-1}	Fitted	
$K_{\text{pde–pve}}$	s^{-1}	$\frac{L_{\text{f}} K_{\text{pde–pve}}}{u_{\text{pde}}} = \frac{L_{\text{f}} K_{\text{pw–pve}}}{u_{\text{pw}}}$	Assumption based on symmetry observed between the convective phases

[a] The correlations came from Lefebvre et al. [8].

tal RPT data. Hydrodynamic parameter values obtained for the convective phases were very close. Therefore, the assumption was made that the dimensionless number representing the ratio of the mass exchange between phases on the convective transport was the same for the two convective phases. The exchange coefficient from the particle downflow-emulsion phase to the vortex-emulsion phase ($K_{\text{pde–pve}}$) was evaluated based on that dimensionless number. In summary, the model had 11 parameters, but only 9 independent parameters due to global mass balance and holdup definition. Only three parameters were fitted.

3.4. Numerical procedure

The fractional step method was used to solve the equation system [18]. Using this method Renou et al. [19] successfully solved a convective/dispersive/reactive system. The fractional step method is robust and stable if the methods used to solve the sub-system are adequate. It consists of separating the equations into sub-systems that can be solved with an efficient numerical method. For each time step, the solution of one sub-system becomes the initial condition of the next sub-system. For example, the convection sub-system of Eq. (4) was solved by simply shifting the matrix index for one time step (using $\Delta z = u_{\text{pwd}}\Delta t$) and the result became the initial condition for calculating the linear ordinary differential equation mass exchange sub-system. That sub-system was solved by the Runge–Kutta method with an adaptable time step. For solving the linear dispersion sub-system of the vortex-emulsion phase, the exponential matrix was used [20].

The fractional step method converges toward a unique solution while decreasing the time step. The method is stable, i.e., the error does not increase with each time step and the solution is consistent with the results (see Section 4). Various discretizations of the velocity distribution function (Eq. (1)) were used in order to converge toward a unique solution. A velocity step of 0.05 m/s is sufficient over a range from 0 to 1.3 m/s. A Nelder–Mead direct search method was used to fit the three parameters. The model was fitted onto various tracer concentration curves along the reactor length. Fitting onto only one curve would have produced various sets of fitted parameters giving the same minimization of the objective function [3].

4. Results and discussion

Fig. 3 shows two examples of calculated data, one for each reactor diameter. The model was fitted simultaneously onto three curves above the region of the tracer injection, i.e., $z > 0.2$ m. The objective function used is shown here:

$$r^2 = \frac{\sum_{j=1}^{j=\text{Nb}_z}\sum_{i=1}^{i=\text{Nb}_t}(C_{\text{s exp}_i} - C_{\text{s mod}_i})_j^2}{\sum_{j=1}^{j=\text{Nb}_z}\sum_{i=1}^{i=\text{Nb}_t}(C_{\text{s exp}_i})_j^2} \quad (10)$$

where "j" represents the tracer concentration curve of the various axial positions, "i" represents the tracer concentration value for a given time; Nb_z and Nb_t are, respectively, the number of axial measurement positions and the number of time steps. This objective function forces the fitting procedure to obtain the parameter set respecting not only a tracer concentration curve at one axial position, but respecting the axial evolution of the tracer concentration curves as proposed by Lefebvre et al. [3].

The increasing rank of difficulty for a model to fit the data is as follows: steady-state axial profile, one residence time distribution (RTD), axial evolution of RTDs or batch tracer curves. In other words, more models can fit a steady-state axial profile better than an evolution of RTDs. A model following the tracer axial evolution would represent the mixing mechanism well [1].

The fit quality for the 0.10 m reactor is good with a normalized square residual (r^2) ranging from 0.004 to 0.023. The fit quality for the 0.292 m reactor is fairly good with r^2 ranging from 0.017 to 0.093. For the larger reactor, the overshoot close to the injection zone is more pronounced due to the higher ratio of the solid circulation velocities to the exchange coefficient ($\phi_{\text{pw}}u_{\text{pw}}/K_{\text{pw–pve}}$). The axial evolution of the overshoot is difficult to fit. This is due to the assumption that the model parameters are not a function of the axial position. The authors' previous work [8] indicated, for example, that the particle wake phase holdup is a parabolic function of the axial position. In order to have a number of parameters as low as possible and because the model captured the trend of the tracer curve evolution, the convective/dispersive model was not updated. The model respected the observed contribution of both the convective and dispersive mixing mechanisms (see Fig. 2). Furthermore, the model gave a good estimation of the solid phase mixing time. Cassanello et al. [10] used a model assuming one velocity for the particles going up and another for the particles going down. Solid particles in the vortex-emulsion phase were not considered. Solid mixing was represented by an exchange coefficient linking the upflow and downflow solid particles. Such a model overpredicted the solid phase mixing time, because it did not take into account the axial mixing.

Table 3 presents the three fitted parameters (u_{pw}, $K_{\text{pw–pve}}$ and $D_{\text{ax}_{\text{pve}}}$) as well as the particle wake phase holdup (ϕ_{pw}) and the STD of the particle wake velocity distribution (σ_{pwd}). The other model parameters may be calculated with the relations given in Table 2. The particle wake phase holdup represents the contribution of the convective mixing mechanism in terms of relative volume of the convective phases (remember that $\phi_{\text{pde}} = \phi_{\text{pw}}/0.90$ as shown in Table 2). The particle wake velocity distribution STD and the axial dispersion coefficient of the vortex-emulsion phase represent, in terms of mixing extent, the contribution of the convective and dispersive mixing mechanism, respectively. The solid phase holdup is also given in Table 3 due to its link with the convective/dispersive model parameters (discussed later).

The axial dispersion model (Eqs. (6) and (7) with $\phi_{\text{pde}} = \phi_{\text{pw}} = 0$) was also fitted onto the tracer curves. That model did not give a good fit quality as shown in Fig. 4. This figure compares the fit quality of the axial dispersion model with the convective/dispersive model at the same operating conditions. The r^2-values for the axial dispersion model are about 2–4 times higher than the r^2-values for convective/dispersive model, except for run 1.

The axial evolution of the tracer curves was badly followed by the axial dispersion model. This means that the solid mixing

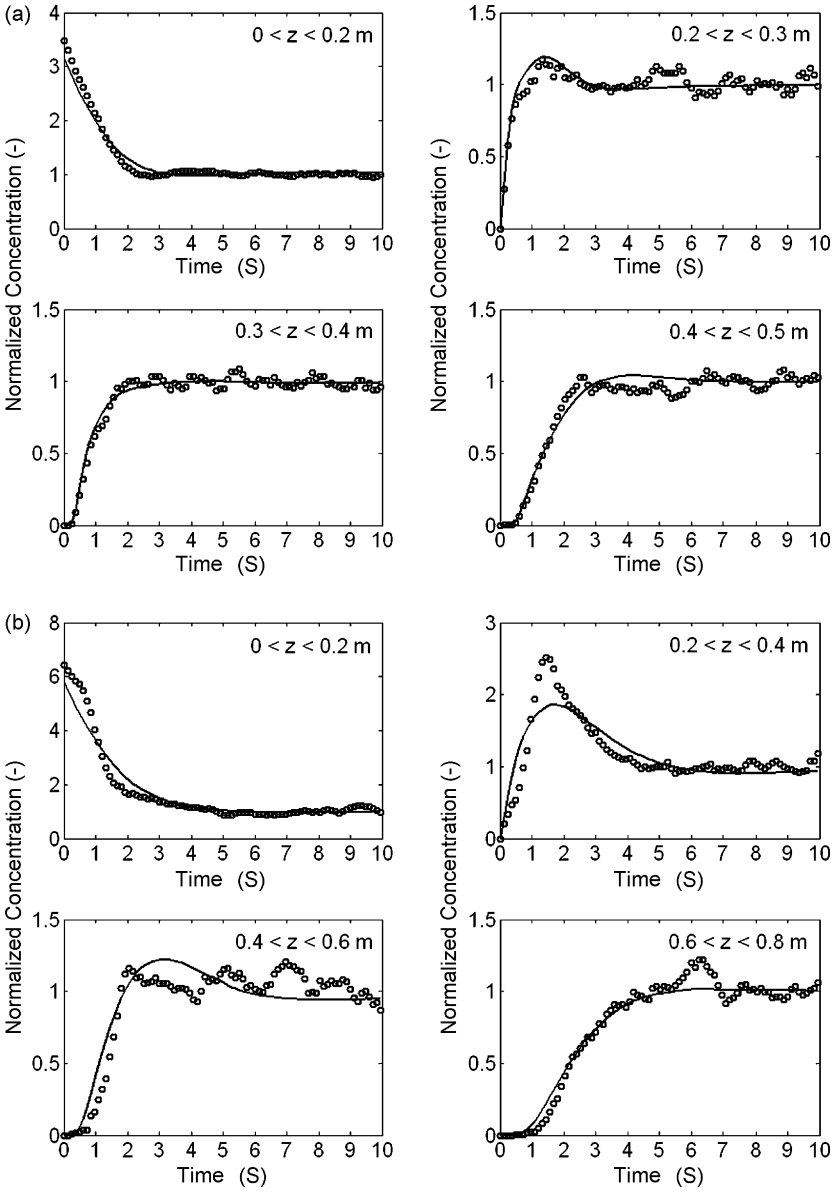

Fig. 3. Convective/dispersive model fitting quality example for GB3mm. (a) $D_c = 0.10$ m, $U_L = 0.065$ m/s, $U_g = 0.106$ m/s. (b) $D_c = 0.292$ m, $U_L = 0.051$ m/s, $U_g = 0.051$ m/s. Dot: experimental result, line: model result.

has to be represented by more than only one parameter. The axial dispersion model is not appropriate as was expected from Cassanello et al. [10], Lefebvre et al. [3] and Lefebvre et al. [8]. The apparent axial dispersion coefficient ($D_{ax_{app}}$) values are shown in Table 3. A comparison of $D_{ax_{app}}$ between the two reactors should be made carefully, because the fit qualities were poor. Although the apparent axial dispersion coefficient is not correct to describe mixing and, especially, to be used to predict reactor conversion and selectivity when the kinetics are fast, it is often used in the literature. The values obtained here are similar with the ones obtained by Fan et al. [21], i.e., 0.005–0.1 m^2/s, for 3 mm glass beads in a three-phase fluidized bed containing a binary system (3–4 and 3–6 mm glass beads).

For most cases, $D_{ax_{pve}} \ll D_{ax_{app}}$ and the extent of mixing is mainly due to the convective mixing mechanism. In other words, the extent of mixing is determined by the standard deviation of the velocity distribution of the convective phases and not by Fick's law. The difference between the two axial dispersion coefficients is more obvious for the larger reactor.

The convective mixing mechanism is more pronounced for the larger reactor, i.e., particle velocity distribution STD and holdup of the convective phases are higher. Knowing that is important for the scale-up of fast reacting systems from lab-scale ($D_c \leq 0.10$ m) to pilot-scale ($D_c \geq 0.3$ m) and from pilot-scale to commercial-scale ($D_c \geq 1$ m). Lefebvre et al. [8] showed quantitative assessment of that scaling effect and proposed a scaling factor named MMI (mixing mechanism indicator). The relative importance of the mixing mechanisms will change at each scale-up step. The proposed model is capable of following this mixing mechanism changes.

As mentioned previously, the mean particle velocity of each convective particle phase was obtained directly from Lagrangian

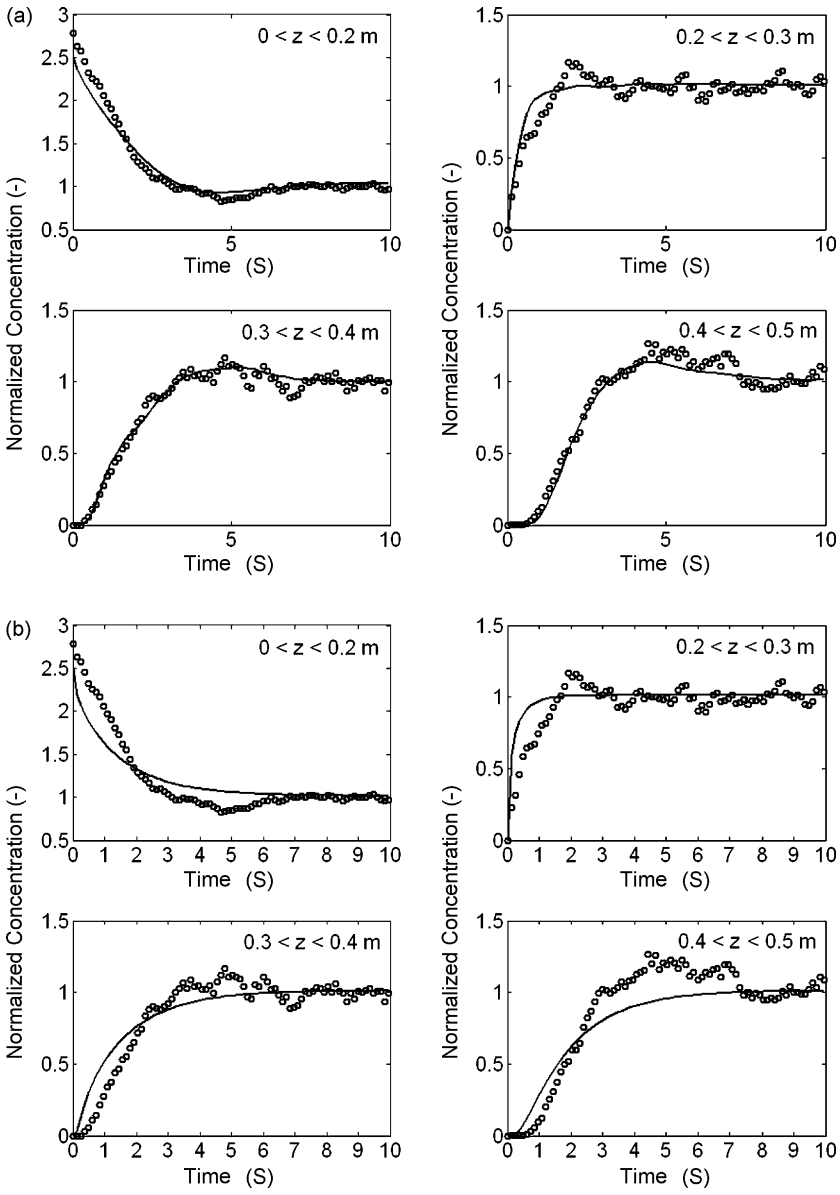

Fig. 4. Convective/dispersive vs. axial dispersion model fitting quality example for GB3mm, $D_c = 0.10$ m, $U_L = 0.065$ m/s, $U_g = 0.069$ m/s. (a) Convective/dispersive model and (b) axial dispersion model. Dot: experimental result, line: model result.

RPT data, i.e., z–t slope of the straight line shown in Fig. 2. As seen in this figure, marked particle paths having constant Lagrangian velocity cover various lengths, called trajectory lengths [22]. The trajectories start and stop at various axial positions. This causes an axial profile of the mean velocity distribution as presented in Fig. 5. The proposed convective/dispersive model assumes that the trajectory lengths are equal to the expanded bed height. Fig. 6 shows that the actual trajectory lengths are much smaller than the expanded bed height and that there is a large distribution of velocities. The proposed model is then a simplification of the reality: particles ascend the bed in the bubble wake, but need various lifts from bubbles to cross the whole height. Between those lifts, the particles spend some time in the vortex-emulsion phase resulting in an apparent lower value of their ascending velocity across the whole bed height. In the experiment presented in Figs. 5 and 6, the average value of the particle velocity across the bed height is 0.29 m/s, while the apparent velocity taking into account the various lifts and the time spent outside of the wakes is 0.24 m/s as obtained by the model. As expected, the apparent velocity is lower (about 20%) than the average velocity (Fig. 7).

The apparent particle wake phase velocity has a tendency to decrease with solid phase holdup. Fig. 8 reflects that tendency. Therefore, the overall solid circulation decreases for systems where the particles are closer. Indeed, the system inertia is higher for larger solid holdup. The particle wake phase velocity is higher in the larger column due to the fastest bubbles being there. The particle wake and particle downflow-emulsion phase velocity distribution STD follow the same trend with the solid phase holdup due to their relation with the particle wake phase velocity. This means that the extent of mixing decreases with the solid phase holdup.

Table 3
Model parameters values and apparent axial dispersion coefficient

Run (#)	ε_s RPT data	ϕ_{pw} RPT data	u_{pw} Fitted (m/s)	σ_{pwd} relation (m/s)	K_{pw-pve} fitted (s^{-1})	$D_{ax_{pve}}$ fitted (m^2/s)	$D_{ax_{app}}$ fitted (m^2/s)
$D_c = 0.10$ m							
1	0.425	0.126	0.07	0.027	0.97	3.29E−2	0.037
2	0.408	0.261	0.15	0.061	0.33	4.44E−2	0.147
3	0.324	0.304	0.28	0.115	1.08	4.79E−12	0.135
4	0.172	0.320	0.22	0.092	0.29	7.85E−12	0.110
5	0.364	0.175	0.13	0.052	0.55	4.15E−2	0.095
6	0.347	0.196	0.20	0.082	1.11	9.34E−3	0.101
$D_c = 0.292$ m							
7	0.503	0.251	0.13	0.077	0.03	2.85E−2	0.037
8	0.459	0.336	0.20	0.121	0.21	4.83E−14	0.074
9	0.459	0.337	0.21	0.126	0.18	2.63E−12	0.096
10	0.485	0.340	0.24	0.146	0.45	2.23E−11	0.071
11	0.451	0.360	0.24	0.144	0.43	5.47E−6	0.073
12	0.451	0.312	0.28	0.165	0.21	1.40E−3	0.111
13	0.436	0.366	0.27	0.162	0.70	2.31E−14	0.076
14	0.436	0.345	0.30	0.177	0.28	2.90E−12	0.117
15	0.436	0.279	0.35	0.169	0.32	2.84E−3	0.133

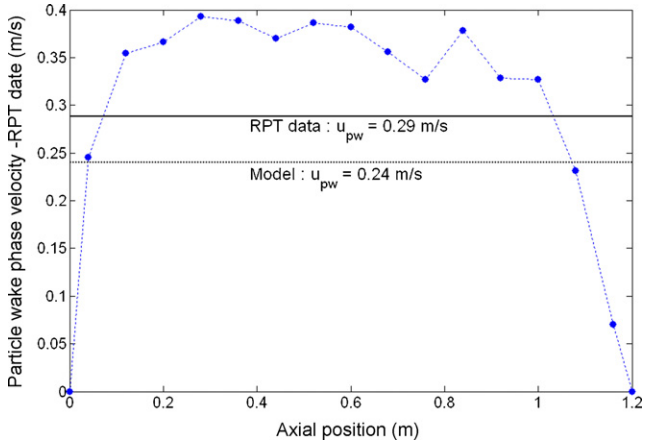

Fig. 5. Axial profile of the mean velocity distribution from RPT data. $D_c = 0.292$ m, $U_L = 0.051$ m/s, $U_g = 0.051$ m/s.

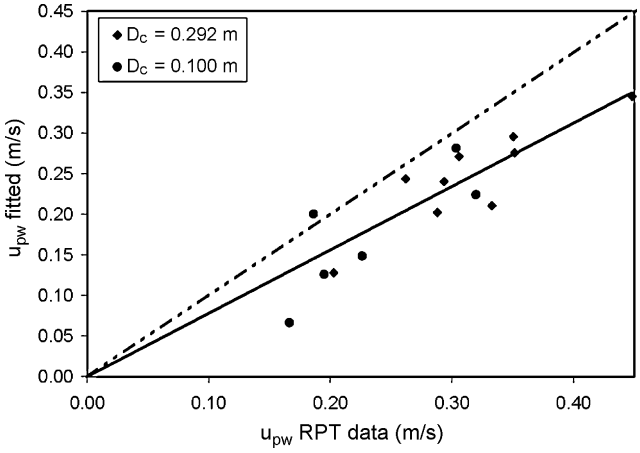

Fig. 7. Particle wake phase velocity—fitted vs. RPT values. The dashed line has a slope of 1. The solid line is a linear fit of the data and the slope is 0.8.

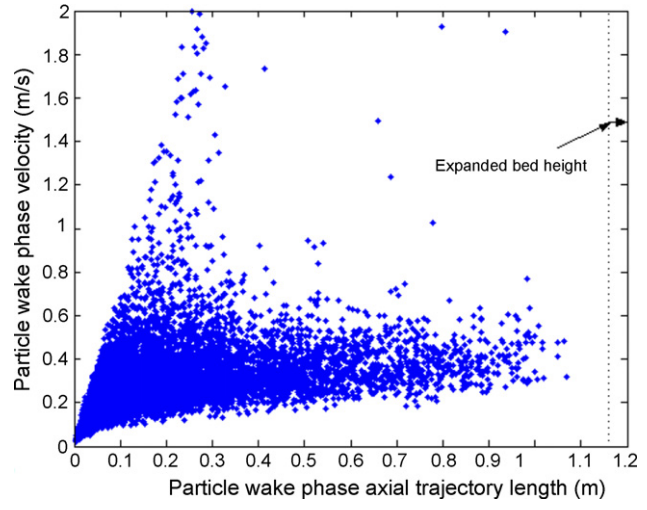

Fig. 6. Particle wake phase Lagrangian velocity (slope of z vs. t) vs. axial trajectory length.

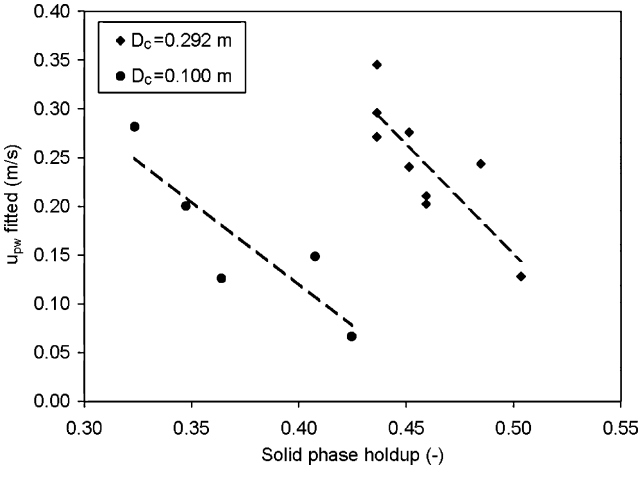

Fig. 8. Fitted particle wake phase velocity vs. solid phase holdup. The dash lines do not represent a correlation, but they only follow the decreasing tendency.

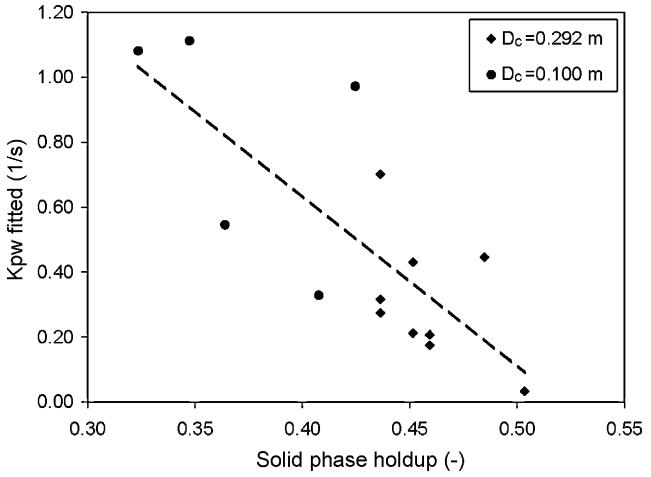

Fig. 9. Fitted exchange coefficient from the particle wake phase to the vortex-emulsion phase vs. solid phase holdup. The dash line do not represents a correlation, but it only follows the decreasing tendency.

The exchange coefficient from the particle wake phase to the vortex-emulsion phase ($K_{pw–pve}$) varied, in a general way, from 0.2 to 1.1 s^{-1}. These values are of the same order of magnitude as the solid mass exchange coefficient obtained by Cassanello et al. [13]. Fig. 9 shows $K_{pw–pve}$ versus the solid phase holdup. This figure reveals a tendency of $K_{pw–pve}$ to decrease with the solid phase holdup. For large solid phase holdup, the particles are closer to each other and their interactions are more pronounced. This stabilizes (retains) the particles in the bubble wake as observed by Fan and Tsuchiya [23] and Fan and Yang [24]. It is demonstrated in Fig. 9 that the exchange $K_{pw–pve}$ is higher for the smaller reactor. Solid particles are exchanged between phases less frequently in a larger reactor. This means that the particle velocity changes less frequently and randomly in larger reactors.

Correlation matrixes of the fitted model parameters were computed at *iso*-r^2. The results indicated weak and very weak correlation between the fitted parameters (from 0.4 to 0.8). This revealed that the fitted parameters are sufficiently independent to represent independent hydrodynamics phenomena.

4.1. Limits of the convective/dispersive model

The relation between the two exchange coefficients shown in Eq. (9) is valid if the solid phase holdup axial profile is flat, as in this case. For slurry reactors and three-phase fluidized beds containing large/light particles, the solid phase holdup changes with the axial position. In that case, the convective/dispersive model may also be applied in the mathematical form given here, but $K_{pw–pve}$ and $K_{pve–pw}$ have to be determined separately. As discussed previously, not taking into account the axial profile of the model parameters reduces the capacity of the model to follow the axial evolution of the tracer concentration curves for the 0.292 m reactor. Moreover, Lefebvre et al. [8] showed that the parameters are also a function of the radial position. The solid particles having a time-averaged upward velocity in the center of the reactor are mostly in the particle wake phase. The solid having a time-averaged downward velocity close the wall (annulus) of the reactor is mostly in the particle downflow-emulsion phase. Between the two regions, the solid is about equally separated between the three particle phases. A more refined model would take into account this spatial repartition of the particle phases.

5. Conclusion

The main objective of this work was to develop a solid phase mixing model that follows not only the mixing extent, but also the overall mixing mechanism, i.e., the contribution of the convective onto the dispersive mixing mechanism. The developed model separates the solid phase into three sub-phases. Two sub-phases follow a convective mixing mechanism and are linked to the bubble velocity distribution. The third sub-phase follows a dispersive mixing mechanism and is subjected to random movement due to drag in the liquid emulsion phase. In the model, the relative contribution of the mixing mechanisms is weighted by the sub-phase holdup, the solid convective sub-phases velocity distribution standard deviation and the axial dispersion coefficient of the dispersive solid sub-phase. Solid mass exchange and overall solid circulation are also considered in the convective/dispersive model. Some model parameters were obtained from the RPT data. Three model parameters were optimized by fitting the convective/dispersive model onto the axial evolution of tracer curves (generated by RPT data). Relations developed in a previous work were used to estimate the remaining model parameters. The model estimated successfully the extent of solid mixing as well as followed the overall mixing mechanism.

In order to develop a predictive model for a three-phase fluidized bed reactor, the next step is to include the model parameters' axial profile functions into the model calculation. A bubble coalescence/breakup model should evaluate these axial profile functions. Local bubble size and bubble velocity distributions would be measured in order to develop a model that will be linked to the solid hydrodynamics in the particle wake phase. Relations found in literature for bubble wake holdup and solid holdup in the wake may be used. The solid hydrodynamics in the particle downflow-emulsion phase may be obtained from relations given by Lefebvre et al. [8]. The solid hydrodynamics in the particle vortex-emulsion phase has to be linked to the liquid phase hydrodynamics. Local measurement in the liquid for a three-phase fluidized bed should be obtained, but it is not an obvious task. There is a great lack of literature for the liquid phase local hydrodynamic in a three-phase fluidized bed.

Acknowledgements

The authors gratefully acknowledge financial support from the Natural Science and Engineering Research Council of Canada and the Fond pour la Fond Québécois de Recherche sur la Nature et la Technologie. Dr. G. Kennedy and Mr. Saint-Pierre are also gratefully acknowledged for activation of the tracer. A special acknowledgement to Pierre Sauriol, who has performed useful modifications to the RPT software system, and to Jean Huard and Robert Delisle, who worked on the experimental setup and RPT facilities.

References

[1] O. Levenspiel, T.L. Fitzgerald, A warning on the misuse of the dispersion model, Chem. Eng. Sci. 38 (1983) 491–493.

[2] O. Levenspiel, Chemical Reaction Engineering, John Wiley & Sons/Oregon State University, 1999.

[3] S. Lefebvre, J. Chaouki, C. Guy, Phase mixing modeling in multiphase reactors containing gas bubble: a review. Int. J. Chem. Reactor Eng. 2 (2004) R2, http://www.bepress.com/ijcre/vol2/R2.

[4] C. Hyndman, C. Guy, Gas phase flow in bubble columns: a convective phenomenon, Can. J. Chem. Eng. 73 (1995) 426–434.

[5] A. Lübbert, B. Larson, Detailed investigations of the multiphase flow in airlift tower loop reactors, Chem. Eng. Sci. 45 (1990) 3047–3053.

[6] F. Larachi, M. Cassanello, J. Chaouki, C. Guy, Flow structure of the solids in a 3D gas–liquid–solid fluidized bed, Am. Inst. Chem. Eng. J. 42 (1996) 2439–2452.

[7] L.S. Fan, Gas–liquid–solid Fluidisation Engineering, Butterworths/Massachusetts Institute of Technology, 1989.

[8] S. Lefebvre, J. Chaouki, C. Guy, Solid phase hydrodynamic of three-phase fluidized bed—a convective/dispersive mixing mechanism representation, Int. J. Chem. Reactor Eng. 5 (2007) A3, http://www.bepress.com/ijcre/vol5/A3.

[9] F. Larachi, M. Cassanello, M.-N. Marie, J. Chaouki, C. Guy, Solids circulation pattern in three-phase fluidized beds containing binary mixtures of particles as inferred from RPT, Trans. Inst. Chem. Eng. 73 (1995) 263–268.

[10] M. Cassanello, F. Larachi, M.-N. Marie, C. Guy, J. Chaouki, Experimental characterization of the solid phase chaotic dynamics in three-phase fluidization, Ind. Eng. Chem. Res. 34 (1995) 2971–2980.

[11] K. Kiared, F. Larachi, C. Guy, J. Chaouki, Trajectory length and residence-time distributions of the solids in three-phase fluidized beds, Chem. Eng. Sci. 52 (1997) 3931–3939.

[12] F. Larachi, G. Kennedy, J. Chaouki, A gamma-ray detection system for 3-D particle tracking in multiphase reactors, Nucl. Instrum. Meth. A338 (1994) 568.

[13] M. Cassanello, F. Larachi, C. Guy, J. Chaouki, Solids mixing in gas–liquid–solid fluidized beds: experiments and modelling, Chem. Eng. Sci. 51 (1996) 2011–2020.

[14] A. Dayan, S. Zalmanovich, Axial dispersion and entrainment of particles in wakes of bubbles, Chem. Eng. Sci. 37 (1982) 1253–1257.

[15] E. Turi, K.M. Ng, Axial distribution of solid particles in bubble column slurry reactors in the bubble flow regime, Chem. Eng. Commun. 46 (1986) 323–345.

[16] W.T. Tang, L.S. Fan, Hydrodynamics of a three-phase fluidized bed containing low-density particles, Am. Inst. Chem. Eng. J. 35 (1989) 355–364.

[17] P. Murray, L.S. Fan, Axial solid distribution in slurry bubble column, Ind. Eng. Chem. Res. 28 (1989) 1697–1703.

[18] N.N. Yanenko, The Method of Fractional Steps: the Solution of the Problems of Mathematical Physics in Several Variables, Springer-Verlag, Berlin, 1971.

[19] S. Renou, M. Perrier, M. Dochain, S. Gendron, Solution of the convection–dispersion-reaction equation by a sequencing method, Comput. Chem. Eng. 27 (2003) 615–629.

[20] W.J. Rugh, Linear System Theory, Prentice Hall Information and System Science Series, Toronto, 1993.

[21] L.-S. Fan, T. Yamashita, R.H. Jean, Solids mixing and segregation in a gas–liquid–solid fluidized bed, Chem. Eng. Sci. 42 (1987) 17–25.

[22] J. Villermaux, Trajectory length distribution (TLD), a novel concept to characterize mixing in flow systems, Chem. Eng. Sci. 51 (1996) 1939–1946.

[23] L.-S. Fan, K. Tsuchiya, Bubble Wake Dynamics in Liquid and Liquid–solid Suspensions, Butterworths/Massachusetts institute of technology, 1990.

[24] L.-S. Fan, G. Yang, Gas–liquid–solid three-phase fluidization. Handbook of fluidization and fluid-particle systems, Y.a.D. Wen-Ching, M, 2002 (Chapter 27).

[25] J.R. Grace, Fluidization, McGraw-Hill, 1982.

[26] L. Schiller, A. Naumann, 1933. Zeitschr, V.D.I. vol. 318-320 (cited by Nigam and Schumpe, 1996).